State-of-the-art model for the LIFES50+ OO-Star Wind Floater Semi 10MW floating wind turbine

Pegalajar Jurado, Antonio Manuel; Bredmose, Henrik; Borg, Michael; Straume, Jonas G.; Landbø, Trond; Andersen, Håkon S.; Yu, Wei; Müller, Kolja; Lemmer, Frank

Published in:
Journal of Physics: Conference Series

Link to article, DOI:
10.1088/1742-6596/1104/1/012024

Publication date:
2018

Document Version
Publisher's PDF, also known as Version of record

State-of-the-art model for the LIFES50+ OO-Star Wind Floater Semi 10MW floating wind turbine

IOP Conf. Series: Journal of Physics: Conf. Series **1104** (2018) 012024 doi:10.1088/1742-6596/1104/1/012024

State-of-the-art model for the LIFES50+ OO-Star Wind Floater Semi 10MW floating wind turbine

Antonio Pegalajar-Jurado[1], Henrik Bredmose[1], Michael Borg[1], Jonas G. Straume[2], Trond Landbø[2], Håkon S. Andersen[2], Wei Yu[3], Kolja Müller[3] and Frank Lemmer[3]

[1] Department of Wind Energy, Technical University of Denmark, Nils Koppels Allé, building 403, DK-2800 Kgs. Lyngby, Denmark

[2] Dr.techn. Olav Olsen AS, Vollsveien 17A, 1366 Lysaker, Norway

[3] Stuttgart Wind Energy, University of Stuttgart, Allmandring 5B, 70569 Stuttgart, Germany

E-mail: ampj@dtu.dk

Abstract.

This paper describes a state-of-the-art model of the DTU 10MW Reference Wind Turbine mounted on the LIFES50+ OO-Star Wind Floater Semi 10MW floating substructure, implemented in FAST v8.16. The purpose of this implementation is to serve as a reference for different activities carried out within the LIFES50+ project. Attention is given to the changes necessary to adapt the numerical model of the onshore DTU 10MW Reference Wind Turbine to a floating foundation. These changes entail controller, tower structural properties, floating substructure hydrodynamics and mooring system. The basic DTU Wind Energy controller was tuned in order to avoid the "negative damping" problem. The flexible tower was extended down to the still water level to capture some of the floater flexibility. The mooring lines were implemented in MoorDyn, which includes dynamic effects and allows the user to define multi-segmented mooring lines. Hydrodynamics were precomputed in the radiation-diffraction solver WAMIT, while viscous drag effects are captured by the Morison drag term. The floating substructure was defined in HydroDyn to approximate the main drag loads on the structure, keeping in mind that only circular members can be modelled. A first set of simulations for system identification purposes was carried out to assess system properties such as natural frequencies and response to regular waves. The controller was tested in a simulation with uniform wind ranging from cut-in to cut-out wind speed. A set of simulations in stochastic wind and waves was carried out to characterize the global response of the floating wind turbine. The results are presented and the main physical phenomena are discussed. The model will form the basis for further studies in the LIFES50+ project and is available for free use.

1. Introduction

In this paper, a state-of-the-art numerical model of the DTU 10MW Reference Wind Turbine (RWT) mounted on the LIFES50+ [1] OO-Star Wind Floater Semi 10MW floating substructure is presented. FAST v8.16, an aero-hydro-servo-elastic numerical tool developed by the National

Renewable Energy Laboratory (NREL), was selected for the implementation of the model. The purpose of this implementation is to serve as a reference for the different activities carried out by partners within the LIFES50+ consortium, in particular:

- Hybrid physical model testing, where a hardware-in-the-loop approach is used to exert rotor loads on a physical model of the floater and turbine tower with a top mass, tested physically in the ocean basin at Sintef Ocean; and where a hardware-in-the-loop controlled hexafoot is used to drive real-time simulated motion of the tower bottom for a physical model of the tower and rotor in the wind tunnel at Politecnico di Milano.
- Model validation, where the accuracy of the state-of-the-art numerical models is screened against experimental results and compared to the performance of simpler models.
- Work related to the model accuracy and its design implications.

The wind turbine structural and aerodynamic models for an onshore configuration have already been implemented in FAST, as described in [2]. In this paper, attention is given to the changes necessary to adapt the FAST model of the onshore DTU 10MW RWT to the floating foundation [3]. These changes entail controller, tower structural properties, floating substructure hydrodynamics and mooring system. First, the wind turbine, the controller and the floating substructure are briefly described in Section 2. Details on the approaches followed to model the wind turbine tower, the mooring system and the floating substructure hydrodynamics are given in Section 3. In Section 4 a selection of load cases is presented, which serves the purpose of testing and demonstrating the numerical model. Results of the simulations are shown in Section 5, along with a discussion of the observed phenomena. Finally, some conclusions are presented in Section 6.

2. Wind turbine and floating substructure

2.1. The DTU 10MW Reference Wind Turbine

The wind turbine employed for the numerical model presented here is the DTU 10MW Reference Wind Turbine, extensively described in [4]. Some key figures are given in Tab. 1 below. To account for the freeboard of the floater and maintain the hub height at 119 m, the turbine tower was shortened, as detailed in [5]. Further, the FAST implementation of the land-based configuration of the DTU 10MW RWT is described in [2].

Table 1. Key figures for the DTU 10MW Reference Wind Turbine [4].

Rated power	Rated wind speed	Wind regime	Rotor diameter	Hub height
10 MW	11.4 m/s	IEC Class 1A	178.3 m	119 m

2.2. The basic DTU Wind Energy controller

The DTU 10MW RWT is here installed on a floating substructure. Therefore, the baseline onshore controller cannot be used here due to the "negative damping" problem (see, for example, [6]). In LIFES50+ the basic DTU Wind Energy controller [7] is employed. The DTU controller consists of two different controllers for the partial load region (i.e. operation below rated wind speed) and the full load region (i.e. operation above rated wind speed), and a mechanism that smoothly switches between these two controllers around rated wind speed. The pole-placement

method [8] was used by Dr.techn. Olav Olsen AS to tune the proportional-integral (PI) controller for the present floating wind turbine configuration. The controller performance will be shown and discussed later in this paper, although details on the controller tuning approach are not within the scope of this paper.

2.3. The OO-Star Wind Floater Semi 10MW floating substructure

The semi-submersible floating substructure (see Fig. 1) was designed by Dr.techn. Olav Olsen AS [9], and its public version is extensively described in [5]. It consists of three outer columns and a central column mounted on a three-legged, star-shaped pontoon with a bottom slab. The main material is post-tensioned concrete. Three catenary mooring lines are employed for station keeping, each with a suspended clump weight. Some of the main properties are collected in Tab. 2 below.

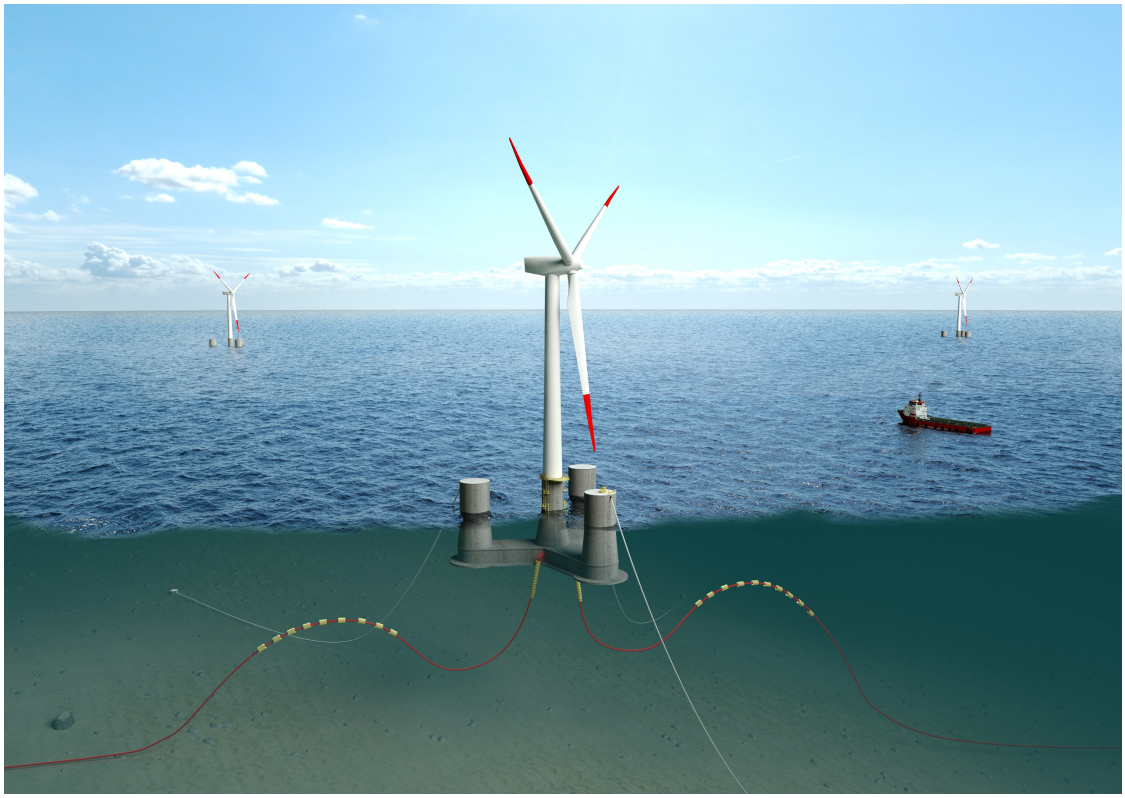

Figure 1. The OO-Star Wind Floater Semi 10MW concept [9].

Table 2. Key figures for the OO-Star Wind Floater Semi 10MW floating substructure.

Water depth	Mooring length	Draft	Freeboard	Displaced volume	Mass incl. ballast
130 m	703 m	22 m	11 m	23509 m^3	21709 t

3. Numerical model

The numerical model was implemented in the aero-hydro-servo-elastic tool FAST v8.16.00a-bjj [10]. FAST (Fatigue, Aerodynamics, Structures and Turbulence), developed at NREL, is an open-source multi-physics tool practical to the engineering design of wind turbines, including both bottom-fixed and floating offshore wind turbines. Only the changes made to the FAST model of the onshore wind turbine [2] will be addressed here. These changes entail modelling of the tower, the mooring system and the hydrodynamics, as well as tuning of the controller. All the information necessary to establish the FAST model was provided by Dr.techn. Olav Olsen AS through [5].

3.1. Modelling of the tower

FAST allows the user to model flexible tower, blades and mooring lines, whereas the floating substructure is modelled as a rigid body (*rigid* approach). Hence, when modelling a floating wind turbine in FAST, it is common practice to model the tower as a flexible beam extending from the nacelle to the interface between the tower and the floater. However, the substructure flexibility is known to have an impact on the system natural frequencies and response (see, for example, [11]). Other aero-hydro-elastic tools include a full structural model of the turbine and floating substructure (*flexible* approach).

To capture some of the floater flexibility, for the model presented here the portion of substructure between still water level (SWL) and tower interface has been modelled as part of the tower (*semi-flexible* approach). This was done by simply extending the definition of the tower to SWL, and by adding one more tower section (tower section 0) to the table of tower properties given in [5]. Table 3 below shows the properties of the added section. For simplicity, the added section has constant diameter, even though the floating substructure has a central column that is tapered from SWL to a height of 2.775 m. However, structural details of the internal design (e.g. wall thickness) are not publicly available and a straight cylinder was used for tower section 0 instead, with the specified values of mass and stiffness properties. This simplification only affects the modelling of the tower, as the tapering of the floater columns is included in the hydrodynamic model.

Table 3. Properties of tower section 0, added to the tower definition in the FAST model.

Height	Outer diameter	Mass density	EA	EI	GJ
11 m	12.05 m	$5.76{\cdot}10^4$ kg/m	$5.96{\cdot}10^{11}$ N	$9.88{\cdot}10^{12}$ Nm^2	$8.23{\cdot}10^{12}$ Nm^2

Since a part of the floating substructure has been modelled as part of the tower, the original inertia properties of the floater need to be modified accordingly (see Fig. 2). The original floating substructure is defined by a mass m_p, a vertical centre of mass CM_p located at a height z_p, a pitch/roll mass moment of inertia I_{yp} and a yaw mass moment of inertia I_{zp}. The portion of floater modelled as tower (tower section 0) has the properties m_0, CM_0, z_0, I_{y0} and I_{z0}. Hence, the new inertia properties for the floating substructure (denoted here with p') can be obtained by solving the equations below, which assure conservation of total mass, centre of mass and mass moment of inertia:

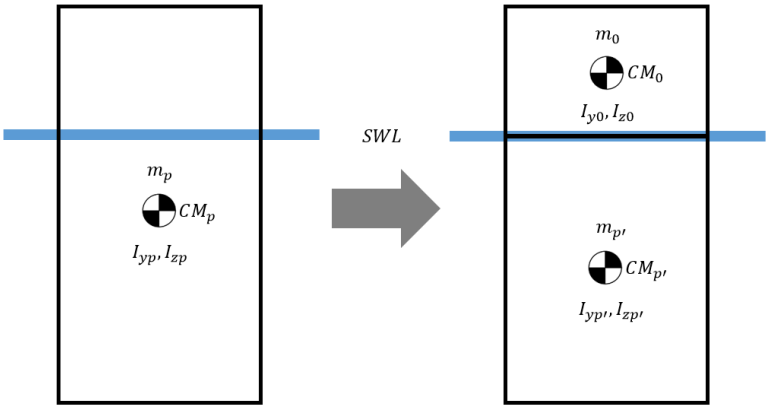

Figure 2. Sketch of the original (left) and modified (right) floating substructure definitions in FAST. In the modified approach, the portion above SWL is modelled as part of the flexible tower.

$$m_p = m_{p'} + m_0, \tag{1}$$
$$m_p z_p = m_{p'} z_{p'} + m_0 z_0, \tag{2}$$
$$I_{yp}^{CM_{p'}} = I_{yp'}^{CM_{p'}} + I_{y0}^{CM_{p'}}, \tag{3}$$
$$I_{zp} = I_{zp'} + I_{z0}. \tag{4}$$

The superscript $CM_{p'}$ indicates that all pitch/roll mass moments of inertia in Eqn. (3) need to be referred to the new floater centre of mass $CM_{p'}$, because the floater mass moment of inertia is given to FAST with respect to the floater CM, which has changed from CM_p to $CM_{p'}$. This can be done by using the parallel axis theorem. For instance, the original floating substructure pitch/roll inertia about the original CM_p can be referred to the new $CM_{p'}$ by virtue of

$$I_{yp}^{CM_{p'}} = I_{yp}^{CM_p} + m_p(z_p - z_{p'})^2. \tag{5}$$

Table 4 below shows the original and the modified floater inertia properties.

Table 4. Original and modified mass properties of the floating substructure for the FAST model.

Property	Mass	CM below SWL	Pitch/roll inertia about CM	Yaw inertia about CM
Original	21709 t	15.225 m	$9.430{\cdot}10^9$ kgm^2	$1.630{\cdot}10^{10}$ kgm^2
Modified	21075 t	15.848 m	$9.133{\cdot}10^9$ kgm^2	$1.628{\cdot}10^{10}$ kgm^2

For the FAST model presented here (*semi-flexible* approach), the mode shapes of the blades were computed in BModes using a cantilever boundary condition [2]. The mode shapes of the tower (including tower section 0) were computed in BModes with a cantilever boundary condition as

well, and with the rotor-nacelle assembly represented by a point mass and inertia. With this approach, the coupled tower natural frequency obtained in FAST was 0.746 Hz. According to [5], the tower natural frequency in FAST is 0.786 Hz considering a completely rigid floating substructure (*rigid* approach). The difference in tower frequency observed between these two FAST models (0.75 Hz vs. 0.786 Hz) is due to the flexibility of the portion of the floater above SWL (tower section 0). If a fully flexible structural model of the whole floating wind turbine is considered (*flexible* approach), the tower natural frequency is reported as 0.56 Hz, obtained with a 3DFloat model. Hence, a closer analysis of the natural frequencies was carried out. Two dominant fore-aft modes were found by eigenvalue analysis in the *flexible* 3DFloat model. These modes are compared in Tab. 5 to the frequencies seen in a spectral analysis of the tower response for a tower decay test in the *semi-flexible* FAST model. From the results, there is thus overall agreement between the natural frequencies observed in the two models. The deviations are likely due to i) floater flexibility; ii) the detection method of natural frequency (eigenanalysis method versus decay test method); and iii) the approach to structural modelling in the two solvers.

Table 5. Mode types and natural frequencies with 3DFloat and FAST models.

	Flexible model		*Semi-flexible* model
Mode	Eigenfrequencies	Mode type	Frequencies in decay test
A	0.56 Hz	Top blade in phase with tower, two lower blades in anti-phase with tower	0.579 Hz
B	0.70 Hz	All blades move collectively, in anti-phase with tower	0.746 Hz

Further, and perhaps linked to these effects, it was found that the two models are dominated by different modes in time-domain simulations. Mode "A" was found to dominate in the 3DFloat *flexible* model, while mode "B" was found to dominate in the *semi-flexible* FAST model. For the FAST model, it was further confirmed that the dominant mode type (the three blades move collectively, in anti-phase with the tower) was consistent with the mode "B" of the 3DFloat model. While the two models were thus found to have quite close natural frequencies, the apparent difference in the dominantly excited mode in time-domain simulations is left for future investigation. In conclusion, caution is necessary in the modelling of the tower-floater coupled frequencies and awareness of the discrepancy between the excited tower modes predicted by the two models is necessary. A difference in tower natural frequency is important since the frequency is a design- and cost driver for the tower design. A wrong determination can thus lead to errors in the fatigue prediction and affect the structural lifetime.

3.2. Modelling of the mooring system

The standard version of FAST includes several options for the modelling of mooring lines [12]. Quasi-static mooring loads can be included with the mooring module MAP++. FEAMooring is able to model dynamic effects such as line mass inertia, buoyancy, and hydrodynamic forces from the Morison equation — assuming still water, but considering the kinematics of the mooring line at each time step. However, FEAMooring does not allow multi-segmented mooring lines or clump weights. The mooring module MoorDyn [13] provides the option of multi-segmented lines and clump weights, necessary for the correct modelling of the mooring system considered here. MoorDyn also captures dynamic effects, but the hydrodynamic loads are also applied to a mooring line moving in still water. Finally, the hydrodynamic loads from incident waves on

the mooring lines can be modelled by using FAST together with the commercial tool OrcaFlex. For the present work, however, to be able to correctly model the multi-segment mooring lines, while still keeping the model open-source, the MoorDyn module was chosen.

3.3. Modelling of the hydrodynamics

When modelling a floating wind turbine in FAST, it is common practice to first compute hydrodynamic properties of the floating substructure in a radiation-diffraction, frequency-domain, potential-flow solver such as WAMIT [14], and to couple these frequency-domain results to the time-domain model through the Cummins equation [15]. These hydrodynamic properties are the hydrostatic restoring matrix $\mathbf{C}_{hst}$, the hydrodynamic added mass matrix $\mathbf{A}(\omega)$ and radiation damping matrix $\mathbf{B}(\omega)$, and the vector of wave diffraction forces $\hat{\mathbf{X}}(\omega)$. The reader should note that added mass, radiation damping and wave diffraction forces depend on the angular frequency ω, and that all properties are computed with respect to the point of flotation. These properties, together with the floater inertia matrix $\mathbf{M}$, the Fourier coefficients for the floater motion in 6 degrees of freedom (DoF) $\hat{\boldsymbol{\xi}}(\omega)$ and the Fourier coefficients of the incident wave surface elevation $\hat{\eta}(\omega)$, define the equation of motion for an unrestrained, floating body in the frequency domain,

$$[-\omega^2(\mathbf{M}+\mathbf{A}(\omega))+i\omega\mathbf{B}(\omega)+\mathbf{C}_{hst}]\hat{\boldsymbol{\xi}}(\omega)=\hat{\mathbf{X}}(\omega)\hat{\eta}(\omega). \tag{6}$$

Further details on the radiation-diffraction theory and its coupling to FAST can be found in [16] and [17], respectively.

3.3.1. Viscous effects

Viscous effects are not captured by potential-flow solvers, therefore they need to be modelled separately within the FAST model. This is usually done by inclusion of the drag term from the Morison equation, which provides the transversal drag force df_{drag} on a cylindrical member section of height dz,

$$df_{drag}=\frac{1}{2}\rho C_D D v_{rel}|v_{rel}|dz. \tag{7}$$

Here ρ is the fluid density, C_D is an appropriate drag coefficient, D is the cylinder diameter, and v_{rel} is the relative velocity between the body and the fluid, projected to the normal of the cylinder axis. Analogously, the axial drag on a circular heave plate is computed as

$$F_{drag,hp}=\frac{1}{2}\rho C_{D_{hp}} A_{hp} v_{rel}|v_{rel}|, \tag{8}$$

where $C_{D_{hp}}$ is a drag coefficient and A_{hp} is the heave plate area, projected on the plane normal to the motion.

When modelling viscous drag in FAST, it is important to consider that HydroDyn only allows the user to define cylindrical members, and that the axial loads applied at the member ends are referred to the member cross-section properties at that particular end. In addition, HydroDyn assumes that the axial drag on a heave plate is modelled with two joints (one at each side of the heave plate), and half of the force given by Eqn. (8) is applied at each side. If only one joint is employed, the axial drag coefficients have to be doubled accordingly. To model viscous drag on the OO-Star Wind Floater Semi 10MW floating substructure, 14 members were defined in

HydroDyn (see Fig. 3), as detailed below. The floating substructure was considered brand new, therefore no marine growth effects were included, although for the design process they must be taken into account.

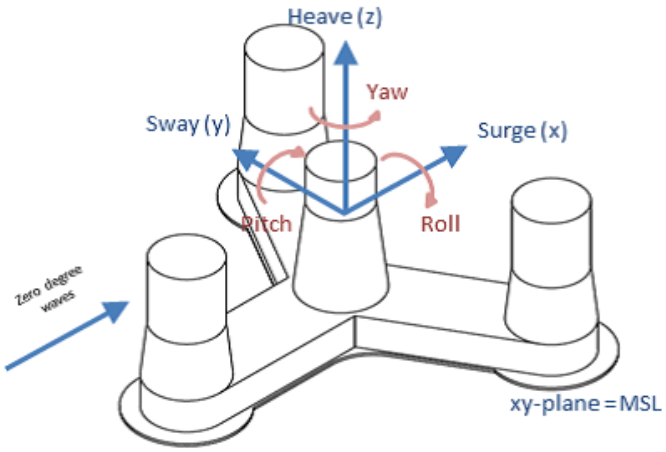

Figure 3. Geometry of the OO-Star Wind Floater Semi 10MW floating substructure.

Central vertical column

- One member corresponds to the upper section of the central column, with a transversal drag coefficient C_D of 0.729 [5] together with the physical column diameter D of 12.05 m.
- One member models the tapered bottom section of the central column, with a variable transversal drag coefficient C_D between 0.729 and 0.704 [5] and a variable diameter D between 12.05 and 16.2 m. This member extends down to the top of the star-shaped pontoon.

Outer vertical columns

- Three members correspond to the upper sections of the three outer columns, with a transversal drag coefficient C_D of 0.720 [5] and the physical column diameter D of 13.4 m.
- Three members represent the tapered bottom sections of the three outer columns, with a variable transversal drag coefficient C_D between 0.720 and 0.706 [5] together with a variable diameter D between 13.4 and 15.8 m. These members extend down to the top of the star-shaped pontoon.
- Three members represent the circular ends of the pontoon legs, with a transversal drag coefficient C_D of 0.706 [5] together with a diameter D of 15.8 m. These members extend from the bottom of the outer tapered columns to the heave plates.

The last three members, which represent the legs of the star-shaped pontoon, are defined to approximate the main drag loads on the physical structure, but taking into account that HydroDyn only allows the definition of cylindrical members. A sketch of the physical and the model representation of the pontoon and slab is presented in Fig. 4. The properties of the cylindrical members and heave plates that represent the star-shaped pontoon and slab in the FAST model are described below and summarized in Tab. 6.

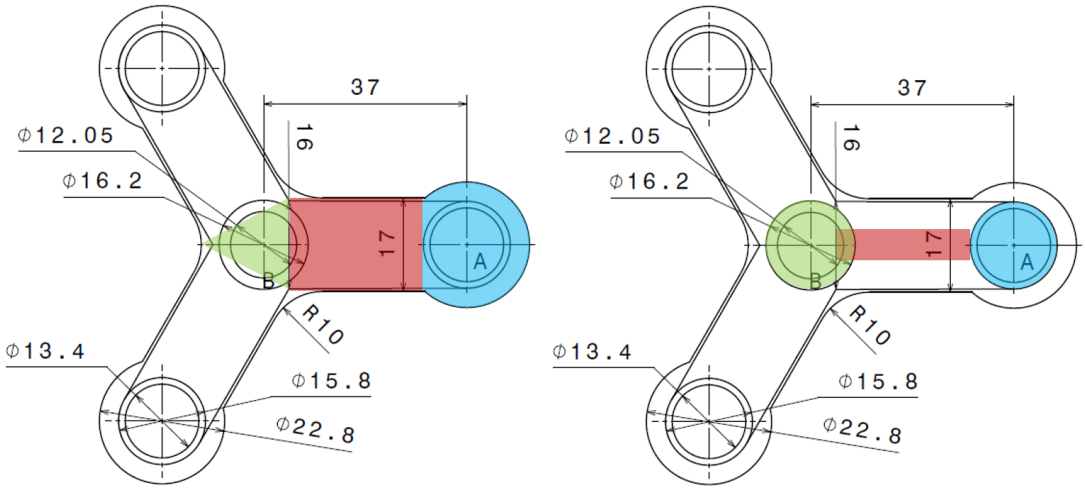

Figure 4. Physical (left) and model (right) representations of the star-shaped pontoon and slab. The dimensions are given in meters.

Outer heave plates (blue)
The heave plate drag coefficient $C_{D_{hp}}$ is taken as 10 from [18], as given in [5]. We note that the value is based on a model scale experiment where the Reynolds number is not identical to the full-scale value. On the other hand, the sharp edge geometry of heave plates is expected to lead to a smaller dependency of the drag coefficient on the Reynolds number. In the LIFES50+ project, physical model tests are carried out which further allows a determination of the floaters damping properties, yet still at model scale. As mentioned before, the axial loads at member ends in FAST are applied to the area of the corresponding member end, therefore the drag on the outer physical heave plate, with drag coefficient $C_{D_{hp}}$ and area A_{hp}, will be applied in the model with a drag coefficient $C_{D_{hp,FAST}}$, scaled to the area of the bottom of the outer column, A_{col}. The resulting values are given in Tab. 6.

Pontoon legs (red)
The pontoon legs in FAST are defined as horizontal cylinders extending from a radial position r_1 of 4.62 m to a radial position r_2 of 29.10 m. This definition of pontoon leaves an "uncovered" central triangle, which is dealt with below. The transverse drag coefficient C_D is taken as 2.05 [5], due to flow separation at the sharp corners. Each physical leg cross-section can be simplified to a rectangle, with height h_1 of 7 m and width h_2 of 17 m (the slight tapering of the pontoon legs is neglected for simplicity). In FAST, each leg is modelled as a cylinder with diameter D equal to h_1. This ensures that the drag in the surge/sway plane will be properly modelled.

Central heave plate (green)
Since the pontoon leg width is more than twice the leg height, the drag loads on the legs in heave and pitch DoFs would be underestimated. To compensate for that, the missing drag was lumped into the three outer heave plates and a central, virtual heave plate (see Fig. 4), which also captures the drag on the green triangle not covered by the pontoon.

To determine the drag coefficients of the heave plates (labeled as $C_{D_{hp0,FAST}}$ for the central heave plate and $C_{D_{hp,FAST}}$ for the outer heave plates), a set of equations was solved. In Eqn. (9), the physical (left-hand side) drag force in heave on one leg of the real structure is equal to the heave force seen by the FAST model (right-hand side). In a similar manner, Eqn. (10) relates the physical drag moment in pitch on one leg to the one seen by the model,

$$\int_{r_1}^{r_2} \frac{1}{2}\rho C_D h_2 \dot{z}|\dot{z}|dr + \frac{1}{2}\rho C_{D_{hp}} A_{hp}\dot{z}|\dot{z}| + \frac{1}{3}\frac{1}{2}\rho C_D A_{tri}\dot{z}|\dot{z}| = \int_{r_1}^{r_2} \frac{1}{2}\rho C_D D\dot{z}|\dot{z}|dr + \frac{1}{4}\rho C_{D_{hp,FAST}} A_{col}\dot{z}|\dot{z}| + \frac{1}{3}\frac{1}{4}\rho C_{D_{hp0,FAST}} A_{col0}\dot{z}|\dot{z}|, \tag{9}$$

$$\int_{r_1}^{r_2} \frac{1}{2}\rho C_D h_2 \dot{\theta}|\dot{\theta}|r^3 dr + \frac{1}{2}\rho C_{D_{hp}} A_{hp}\dot{\theta}|\dot{\theta}|R^3 = \int_{r_1}^{r_2} \frac{1}{2}\rho C_D D\dot{\theta}|\dot{\theta}|r^3 dr + \frac{1}{4}\rho C_{D_{hp,FAST}} A_{col}\dot{\theta}|\dot{\theta}|R^3. \tag{10}$$

Here r is the radial coordinate measured from the centre of the floater, $\dot{z}$ is the heave velocity, $\dot{\theta}$ is the pitch velocity, A_{tri} is the triangular area and A_{col0} is the area of the bottom of the central column. The last term on the left-hand side of Eqn. (9) is the drag on the central triangle, while the last term on the right-hand side is the contribution from the virtual central heave plate, necessary to correctly model the drag in the heave direction. For simplicity, only drag due to floater motion was considered in Eqs. (9) and (10) — i.e. no wave kinematics were included. Also, the contribution of the central triangle to Eqn. (10) was neglected. The two equations were solved simultaneously to yield values of 38.34 for $C_{D_{hp,FAST}}$ and 14.99 for $C_{D_{hp0,FAST}}$. These axial drag coefficients are doubled, because only one joint per heave plate was employed here, contrary to HydroDyn's assumption of two joints per heave plate. A summary of the physical and model properties involved in the viscous drag on the bottom slab of the floating substructure is given in Tab. 6 below.

Table 6. Summary of drag properties for the pontoon and slab of the OO-Star Wind Floater Semi 10MW floating substructure. The values on the middle column have been determined to match the global drag in surge, heave and pitch for the physical structure.

Property	Physical value	Model value	Color in Fig. 4
Pontoon leg height	7 m	7 m (diameter)	
Pontoon leg width	17 m	7 m (diameter)	Red
Pontoon leg drag coeff.	2.05	2.05	
Outer heave plate area	368.57 m^2	196.07 m^2	Blue
Outer heave plate drag coeff.	10.00	38.34	
Central heave plate area	125.14 m^2 (triangle)	206.12 m^2	Green
Central heave plate drag coeff.	2.05	14.99	

4. Selection of load cases

A set of representative load cases from [19] was selected with the purpose of demonstrating the numerical model. In Tab. 7 below, cases 1-8 (system identification) are of diagnostic nature, while load cases 9-15, 16-17 and 18 (response to wind and waves) are representative of Design Load Case (DLC) 1.2, 1.6 and 6.1, respectively. As specified in [19] for the Gulf of Maine, for load cases 9-18 the wind turbulence was set to Class C, and a Pierson-Moskowitz spectrum was

Table 7. Summary of load cases simulated with the FAST model.

No.	Description	Time [s]	Waves	Wind	Wind turbine
1	Static equilib.	1000	-	-	Parked
2	Surge decay	1000	-	-	Parked
3	Heave decay	1000	-	-	Parked
4	Pitch decay	1000	-	-	Parked
5	Yaw decay	1000	-	-	Parked
6	Tower decay	1000	-	-	Parked
7	Regular wave	1800	Reg, 6.00 m, 10.0 s	-	Parked
8	Step wind	15000	-	St+unif, 4-25 m/s	Operating
9	Operational 1	5400	Irreg, 1.38 m, 7.0 s	Turb, 5.0 m/s	Operating
10	Operational 2	5400	Irreg, 1.67 m, 8.0 s	Turb, 7.1 m/s	Operating
11	Operational 3	5400	Irreg, 2.20 m, 8.0 s	Turb, 10.3 m/s	Operating
12	Operational 4	5400	Irreg, 3.04 m, 9.5 s	Turb, 13.9 m/s	Operating
13	Operational 5	5400	Irreg, 4.29 m, 10.0 s	Turb, 17.9 m/s	Operating
14	Operational 6	5400	Irreg, 6.20 m, 12.5 s	Turb, 22.1 m/s	Operating
15	Operational 7	5400	Irreg, 8.31 m, 12.0 s	Turb, 25.0 m/s	Operating
16	Ultimate 1	5400	Irreg, 10.90 m, 16.0 s	Turb, 7.1 m/s	Operating
17	Ultimate 2	5400	Irreg, 10.90 m, 16.0 s	Turb, 22.1 m/s	Operating
18	Extreme	5400	Irreg, 10.90 m, 16.0 s	Turb, 44.0 m/s	Parked+fth

used for the irregular sea states. These load cases were run for 5400 s to be able to remove 1800 s of transient (given the long surge natural period for this floating substructure, see Tab. 9), and the turbulence boxes had a duration of 5400 s as well. The wave conditions for load cases 16-18 correspond to the 50-year significant wave height and the upper limit of the 50-year peak period range [19]. In Tab. 7, the wave parameters indicate wave height H and period T for regular wave "Reg", while they refer to significant wave height H_s and peak period T_p for irregular sea states "Irreg". The wind speed values refer to the mean wind speed at hub height, both for steady, uniform wind "St+unif" and turbulent wind "Turb". The wind turbine is parked (i.e. fixed rotor) for the cases with no wind and operating with active control otherwise — except for case 18, where it is parked and the blades are in feather position, "Parked+fth".

5. Results

5.1. System identification

5.1.1. Static equilibrium

A first simulation with no wind, no waves and no initial displacements was run to assess model stability and correct balance between gravitational and buoyancy forces. Due to imperfect balance between global weight and net buoyancy, and to the tower-top CM not being aligned with the tower axis, a small offset was observed in surge, heave and pitch (see Tab. 8). This offset was used as initial condition in all the simulations to reduce the transient time.

5.1.2. Free decays

Free decay simulations were carried out in the FAST model, where for each decay case, an initial displacement was introduced in the corresponding DoF and the system was left to decay

Table 8. Static offsets in the FAST model.

Surge	Heave	Pitch
0.112 m	0.054 m	-0.233 deg

to its equilibrium position. A Fourier analysis of the relevant time series revealed the natural frequencies involved, as well as couplings between DoFs and the level of damping. The initial displacement chosen is representative of the given DoF. The tower decay was carried out with all floater DoFs active. The natural frequencies and periods are presented in Tab. 9.

Table 9. System natural frequencies and periods from decay simulations in FAST.

Surge	Heave	Pitch	Yaw	Tower
0.0054 Hz	0.0478 Hz	0.0316 Hz	0.0097 Hz	0.746 Hz
185.19 s	20.92 s	31.65 s	103.09 s	1.34 s

5.1.3. Response to regular waves

The model response to a regular wave with no wind is useful to assess whether the hydrodynamic loads are properly modelled. The response to a regular wave with $H = 6$ m and $T = 10$ s is shown in Fig. 5, where the first 1200 s have been discarded in the power spectral density (PSD) analysis due to transient effects. It is observed that the motion is dominated by the wave frequency at 0.1 Hz for all DoFs. The thrust signal shows some periodic variations, because it does not refer to purely aerodynamic thrust here, but instead it refers to the force felt along the low-speed shaft, which also contains some inertia components.

5.1.4. Response to step uniform wind

The controller was tested by simulating a case with no waves and uniform, steady wind speed that goes from cut-in wind speed at 4 m/s to cut-out at 25 m/s, changing in intervals of 1 m/s every 10 min (see Fig. 6, where the first 1800 s have been excluded from the plots). Every time the wind speed is increased, the thrust on the rotor changes and the floating substructure moves to its new equilibrium position, describing oscillations around it that decay with time. These oscillations happen at the natural frequency in each DoF. Because this floating substructure has long natural periods, the structure is still oscillating when the wind speed is changed again, as seen especially for surge. It can be seen that the controller is able to maintain floater pitch stability for all wind speeds in the test. An important observation here is that the surge motion seems to be less damped for wind speeds between 11.4 and 16 m/s, although the controller was tuned to provide positive damping in pitch in the full-load region. Further investigations revealed that, due to the controller, the aerodynamic damping in surge is negative or zero for these wind speeds. However, in real environmental conditions (i.e. wind and waves), we observed that the hydrodynamic damping contributes to a positive global damping of the surge mode. In the case shown in Fig. 6, since no waves are present, the effect of the aerodynamic damping in surge is more visible. This controller effect is similar to the negatively-damped pitch motion reported in [6]. A solution similar to the one proposed in [6] would entail tuning the controller so its natural frequency is below the floater's surge natural frequency. This approach, however, would significantly affect the wind turbine power production. Since the surge global damping has been

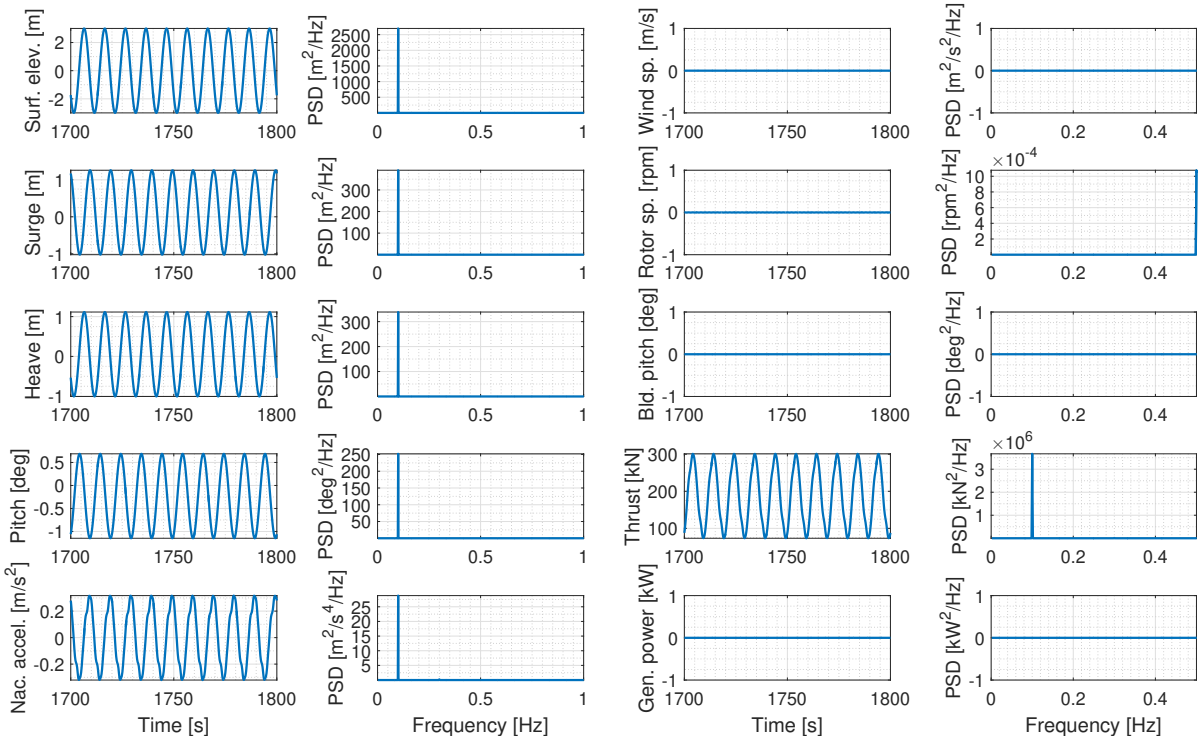

Figure 5. Response to regular waves, load case 7.

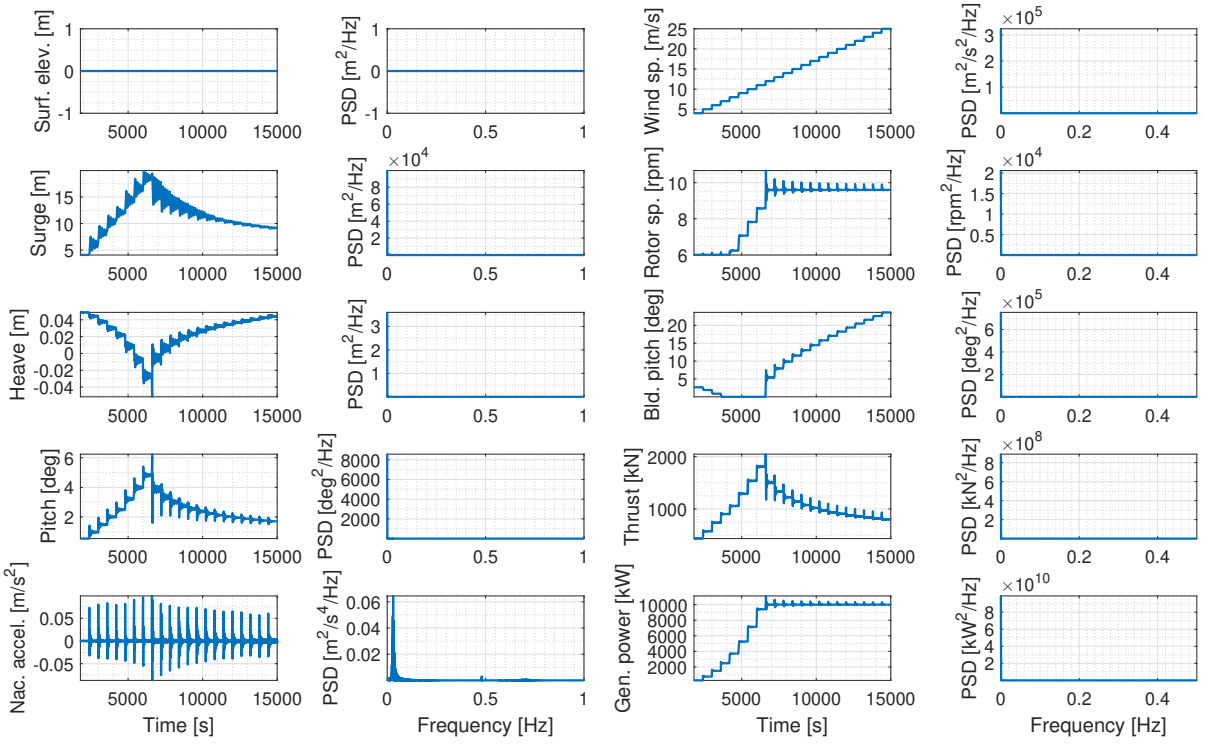

Figure 6. Response to step wind, load case 8.

observed to be positive in real-life environmental conditions due to hydrodynamic effects, this action is not recommended. Exploitation of further control strategies can likely lead to improved performance and is left for future work.

5.2. Response to wind and waves

5.2.1. Operational conditions

Figure 7 shows the response to irregular waves and turbulent wind in operational conditions. The load case is number 12 in Tab. 7, with $V = 13.9$ m/s, $H_s = 3.04$ m and $T_p = 9.5$ s. The first 1800 s have been excluded from the PSD analysis to discard transient effects. The surge and pitch motions are dominated by the surge and pitch natural frequencies respectively, likely excited by the wind forcing. The heave motion, on the other hand, is dominated by wave forcing. The nacelle acceleration shows response mainly at the wave frequency range, but also at the pitch frequency and at the tower natural frequency. The turbine operates as expected with respect to rotor speed, blade pitch and generator power.

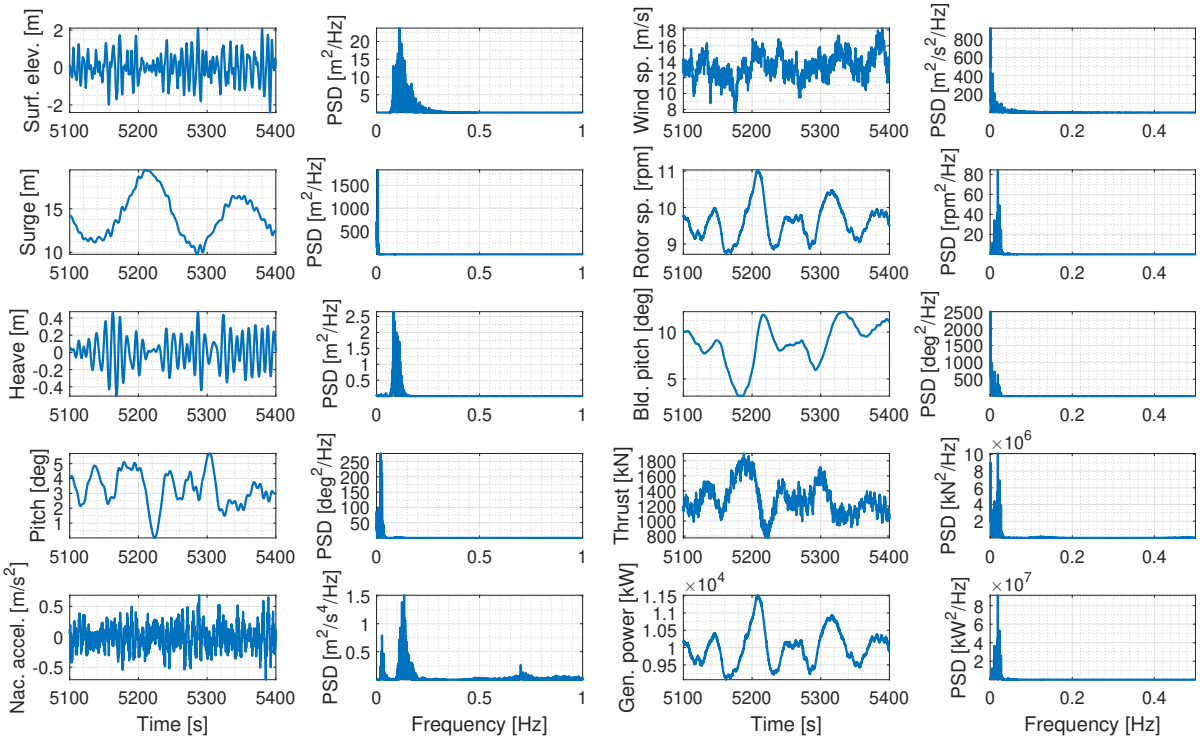

Figure 7. Response to wind and waves, load case 12.

5.2.2. Ultimate conditions

Figure 8 shows the response to irregular waves and turbulent wind in ultimate conditions. The load case is number 17 in Tab. 7, with $V = 22.1$ m/s, $H_s = 10.9$ m and $T_p = 16$ s (50-year sea state). The first 1800 s have been excluded from the PSD analysis. In this case the wave forcing dominates most of the floater motions, although the wind forcing also seems to excite the natural frequencies of the surge and pitch modes. As in the case presented in Fig. 7, the PSD of nacelle acceleration shows some minor energy at the coupled tower natural frequency. Once again, the turbine operates normally in terms of rotor speed, blade pitch and generator power.

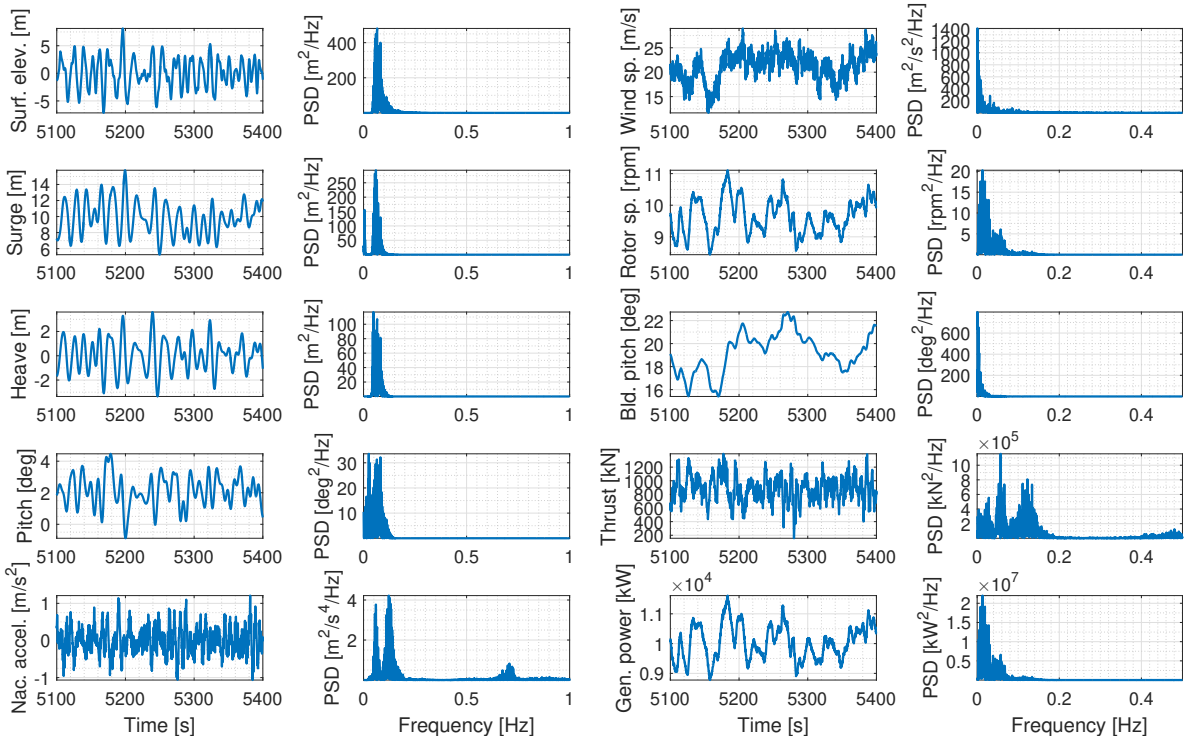

Figure 8. Response to wind and waves, load case 17.

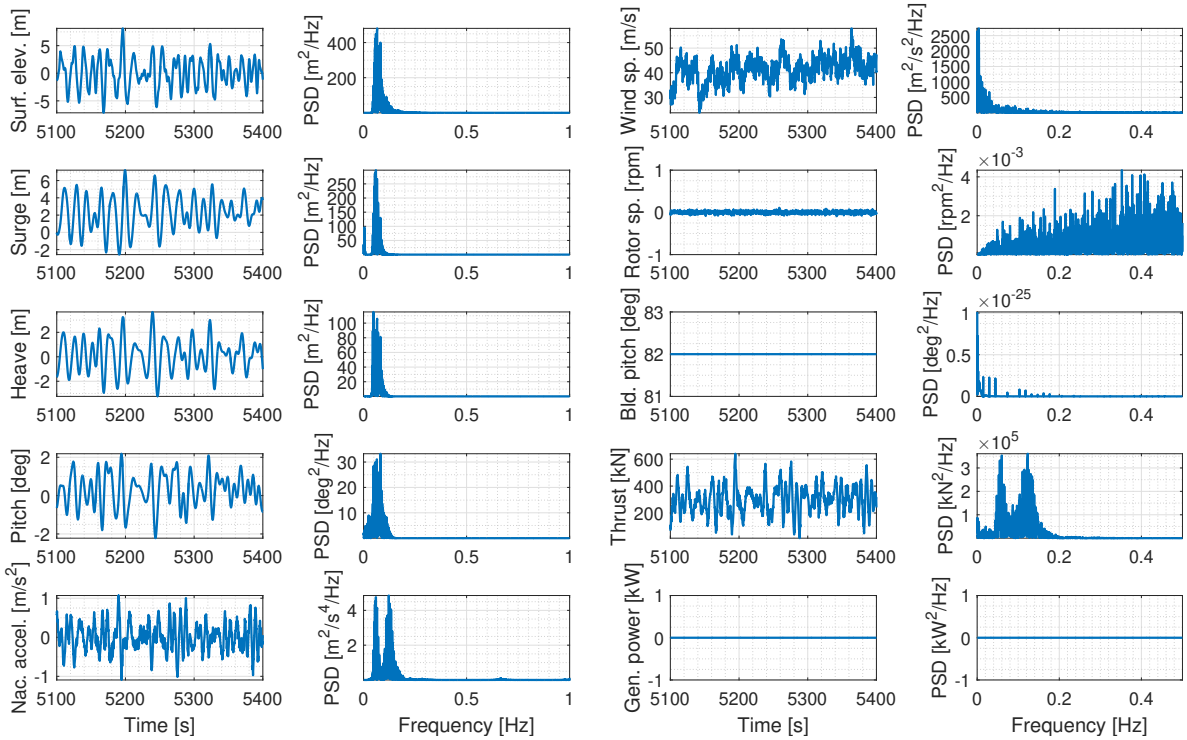

Figure 9. Response to wind and waves, load case 18.

5.2.3. Extreme conditions

Figure 9 shows the response to irregular waves and turbulent wind in extreme conditions. The load case is number 18 in Tab. 7, with $V = 44$ m/s, $H_s = 10.9$ m and $T_p = 16$ s. The first 1800 s have been excluded from the PSD analysis to discard transient effects. The difference between this case and the one presented in Fig. 8 is that the wind speed is here 44 m/s and therefore the turbine is parked, with the blades in feather position. The responses are solely wave-dominated in this case, given that the aerodynamic forces on the rotor are significantly smaller, and drag loads on the tower are not included. However, some wind-induced surge motion can still be observed. The response of the nacelle at the coupled tower frequency is not visible anymore, which indicates it was due to the wind.

6. Conclusions

We have presented the implementation in FAST of the DTU 10MW RWT mounted on the LIFES50+ OO-Star Wind Floater Semi 10MW floating substructure. FAST v8.16 was selected as the version for implementing the numerical model. Attention was given to the changes necessary to adapt the FAST model of the onshore DTU 10MW RWT to the floating foundation. These changes entail controller, tower structural properties, mooring system and floating substructure hydrodynamics. The portion of the floater above still water level was included in the flexible modelling, and comparison to a fully flexible model of the turbine configuration was made. With this approach the two dominant tower modes of the flexible model were reproduced in the FAST model with quite close natural frequencies. A difference, however, as to which of these modes was dominantly excited in time-domain simulations was found and discussed. The viscous effects on the physical pontoon and heave plates were modelled by a combination of cylindrical members and heave plates, adjusted to yield the correct physical drag forcing in surge, heave and pitch. A first set of simulations for system identification purposes was carried out to assess system properties such as static offset, natural frequencies and response to regular waves. The controller was tested in a simulation with uniform wind ranging from cut-in to cut-out wind speed. A set of simulations in stochastic wind and waves was carried out to characterize the global response of the floating wind turbine. The model will form the basis for further studies in the LIFES50+ project and is available for free use.

Model availability and referencing

The FAST model and the simulation results presented here are freely available to the public at `https://rwt.windenergy.dtu.dk/dtu10mw`. In the event of publication of work resulting from the use of the model, appropriate referencing to [3], [5] and this paper should be included.

It is noted that although the public design which the present model is based on may have similarities with real commercial designs, its specifications can by no means be taken as confirmed values for any commercial design. It is expected, though, that the public model will be of benefit for wider research on floating wind turbines due to its open specification.

Acknowledgements

This work is part of the LIFES50+ project [1]. The research leading to these results has received funding from the European Union's Horizon 2020 research and innovation programme under grant agreement No. 640741. Also, the authors are grateful to Dr.techn. Olav Olsen AS [9] for the permission and contribution to set up the present numerical model based on their concept of the OO-Star Wind Floater Semi 10MW.

References

[1] LIFES50+ project URL http://lifes50plus.eu/
[2] Borg M, Mirzaei M and Bredmose H 2015 LIFES50+ D1.2: Wind turbine models for the design Tech. rep. Technical University of Denmark
[3] Pegalajar-Jurado A, Madsen F, Borg M and Bredmose H 2018 LIFES50+ D4.5: State-of-the-art models for the two LIFES50+ 10MW floater concepts Tech. rep. Technical University of Denmark
[4] Bak C, Zahle F, Bitsche R, Kim T, Yde A, Henriksen L, Natarajan A and Hansen M 2013 Description of the DTU 10 MW reference wind turbine Tech. rep. No. I-0092, DTU Wind Energy
[5] Yu W, Müller K and Lemmer F 2018 LIFES50+ D4.2: Public definition of the two LIFES50+ 10MW floater concepts Tech. rep. University of Stuttgart
[6] Larsen T and Hanson T 2007 *Journal of Physics: Conference Series* **75**
[7] Hansen M and Henriksen L 2013 Basic DTU Wind Energy controller Tech. rep. No. E-0028, DTU Wind Energy
[8] Hansen M, Hansen A, Larsen T, Øye S, Sørensen P and Fuglsang P 2005 Control design for a pitch-regulated, variable-speed wind turbine Tech. rep. No. Risø-R-1500(EN), Risø National Laboratory
[9] Dr.techn. Olav Olsen AS URL http://www.olavolsen.no/
[10] Jonkman J and Jonkman B 2016 NWTC Information Portal (FAST v8) URL https://nwtc.nrel.gov/FAST8
[11] Borg M, Hansen A and Bredmose H 2016 *Journal of Physics: Conference Series* **753**
[12] Wendt F, Robertson A, Jonkman J and Andersen M 2016 *Proceedings of the 26th International Offshore and Polar Engineering Conference (ISOPE 2016)*
[13] Hall M 2017 MoorDyn URL http://www.matt-hall.ca/moordyn.html
[14] Lee C and Newman J 2016 WAMIT URL http://www.wamit.com/
[15] Cummins W 1962 *Schiffstechnik* **9** 101–109
[16] Newman J 1980 *Marine hydrodynamics* 3rd ed (The MIT Press)
[17] Jonkman J 2009 *Wind Energy* **12** 459–492 ISSN 10954244
[18] Tao L and Dray D 2008 *Ocean Engineering* **35** 1006–1014
[19] Krieger A, Ramachandran G, Vita L, Gómez-Alonso G, Berque J and Aguirre G 2015 LIFES50+ D7.2: Design basis Tech. rep. DNV-GL